



MIP-type organic solar cells incorporating phthalocyanine/fullerene mixed layers and doped wide-gap transport layers

J. Drechsel^{a,*}, B. Männig^a, D. Gebeyehu^a, M. Pfeiffer^a, K. Leo^a, H. Hoppe^b

^a Institut für Angewandte Photophysik, Technische Universität Dresden, D-01062 Dresden, Germany

^b Linz Institute for Organic Solar Cells (LIOS), Physical Chemistry, University Linz, A-4040, Linz, Austria

Received 21 August 2003; accepted 18 November 2003

Available online 13 December 2003

Abstract

We describe a simple organic solar cell structure that allows to study in detail loss mechanisms due to non-ohmic contacts, structural drawbacks and material selection: the MIP-type (metal-intrinsic-p-doped) structure discussed here represents the p-side and the active layer within a PIN type solar cell architecture. We here adapt the bulk hetero-junction concept using blends of zinc-phthalocyanine (ZnPc) and buckminsterfullerene C₆₀. Furthermore, we use doped wide-gap materials as hole transport layers that enable a more sophisticated solar cell development. The samples are characterized by combination of current voltage characteristics, impedance spectroscopy and capacitance–voltage measurements. We present an evolution of MIP-type structures which improves all solar cell parameters; in particular, excessive series resistance and contact problems reducing the fill factor could be almost completely eliminated.

© 2003 Elsevier B.V. All rights reserved.

PACS: 72.80.Le; 73.50.Pz; 72.40.+w

Keywords: Organic solar cell; Wide-gap transport layers; Capacitance–voltage; Impedance spectroscopy; Donor–acceptor blend; Zinc-phthalocyanine; C₆₀

1. Introduction

Organic semiconducting materials are currently regarded as a promising alternative in the field of photovoltaics, particularly for large-area solar cells [1]. The main advantages are the flexibility and the potentially low cost production involving

exclusively low temperature processes. The continuous efficiency improvements that have been achieved recently [2–5] are encouraging from both research and applications perspectives.

Our basic approach to organic solar cells is based on small molecule physical vapor deposited multilayer structures. Many single or multilayer structures have been proposed so far by several groups [2,4,6–8]. Depending on materials and layer sequences, power efficiencies of up to 3.6% have been achieved [4,5]. A major problem, however, is the rather poor transport capabilities of the typically undoped materials. Gaseous doping with

* Corresponding author. Tel.: +49-35146335117; fax: +49-35146337065.

E-mail addresses: drechsel@iapp.de (J. Drechsel), pfeiffer@iapp.de (M. Pfeiffer).

URL: <http://www.iapp.de>.

e.g. oxygen or bromine [9–12] improves the conductivity for hole transport materials, but are not the method of choice for stable and reproducible device performance. A further problem is that the absorbing materials are also used for charge transport layers. Excitons or charge carriers created close to the metal electrode undergo a quenching process [13] and therefore cannot contribute to the photocurrent. To overcome this problem, it is our approach to introduce wide-gap transport layers to create a spacer layer in between.

In Fig. 1(a), the general structure of a PIN type organic solar cell (OSC) including doped wide-gap transport materials is shown. This approach has a number of advantages:

1. The transport layers are doped in order to increase the conductivity and thus reduce the ohmic losses.
2. Quenching processes at the electrode can be avoided because excitons created in the active layer cannot penetrate into the wide-gap transport layers.
3. The thickness of the highly conductive spacer layers can be tuned to optimize the optical field distribution in the solar cell.
4. The increased overall thickness of the devices allows higher stability and a lower probability for short cuts.

All these arguments apply in a similar way to organic light emitting diodes (OLEDs). Accord-

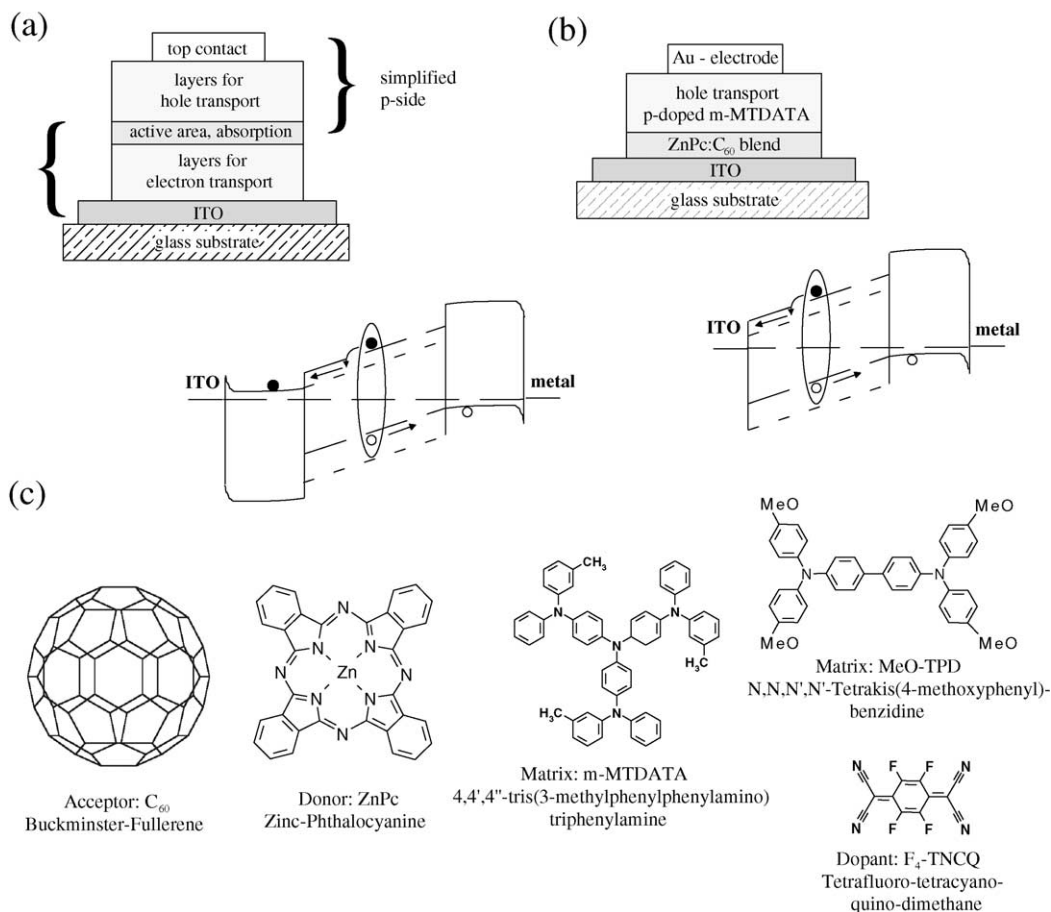


Fig. 1. General structure and schematic illustration of the energy level alignment of a PIN-type organic solar cell (a) and the basic sample structure of the investigated cells (b). Chemical structures of all used materials (c).

ingly, the PIN concept using doped wide-gap transport layers has already been used by our group to demonstrate low voltage, high efficiency OLEDs [14–17].

It is obvious that the PIN concept leads to a rather complex cell structure. To improve the understanding of this type of cell, we investigate in this paper a selected part of the PIN structure: we choose one half of the PIN structure with a metal Schottky contact to study the interplay of n- or p-side with the active layer and the contacts. We would like to stress here that we do not intend to achieve the best overall solar cell performance. We rather show an evolution of a simple structure towards an optimized building block that can be introduced into a final solar cell structure.

The focus of this work is dedicated to the p-side (hole transporting side) of a final organic PIN photovoltaic cell. We are using the already known bulk hetero-junction concept as an active layer which consists of a mixture of zinc-phthalocyanine (ZnPc) and the well known fullerene (C_{60}). Former publications [18–20] have shown the outstanding absorption and charge carrier generation properties of this concept. Excitons created on the ZnPc undergo a fast charge separation, thereby transferring an electron to the C_{60} . The charge separated state of the solid can live up to milliseconds [21] which provides ample time for the charges to dissociate and move to the respective contacts.

2. Experiment

All samples are prepared on $25 \times 25 \text{ mm}^2$ indium tin oxide coated glass substrates (Thin Film Devices Inc., sheet resistance $< 80 \Omega/\square$) that were prestructured and cleaned by a standard procedure resulting in three devices with an average active sample area of about $3\text{--}4 \text{ mm}^2$. Organic layers have been deposited in an UHV multichamber system with a base pressure of typically 10^{-8} mb . In Fig. 1(b), the basic sample structure is shown. As the absorbing and photoactive layer, a one by one mixture of zinc-phthalocyanine (by Syntec GmbH, Wolfen) and fullerene (C_{60} by Kurchatov Institute, Moscow) is used followed by a hole transport layer made of 4,4',4''-tris(3-methyl-phenyl-phenyl-amino)triphenylamine (m-MTDATA

by Syntec GmbH, Wolfen) or *N,N,N',N'*-tetraakis(4-methoxyphenyl)-benzidine (MeO-TPD by Syntec GmbH, Wolfen) doped by the strong acceptor molecule tetrafluoro-tetracyano-quinodimethane (F_4 -TCNQ by Acros Organics). Typical doping concentrations are 2–4 mol%. Those hole transport materials were already successfully applied in OLEDs [14–17]. Details about the doping mechanism can be found in [22–24]. All materials (except F_4 -TCNQ) were purified twice by vacuum gradient sublimation prior to evaporation. Additionally, m-MTDATA and MeO-TPD, showing a liquid phase, have been zone refined about 100 times. All measurements were done in vacuum or in inert nitrogen atmosphere. Illumination was applied by a standard halogen bulb with various light intensities (1/1000 sun to 1 sun) using neutral density filters. The results are based on a series of current–voltage (*IV*), impedance (*IS*) and capacitance–voltage (*CV*) measurements in the dark and partly under illumination.

To monitor the evaporation process of the samples, we routinely measure the lateral current between two contacts on one substrate during layer growth. In Fig. 2, two typical examples of

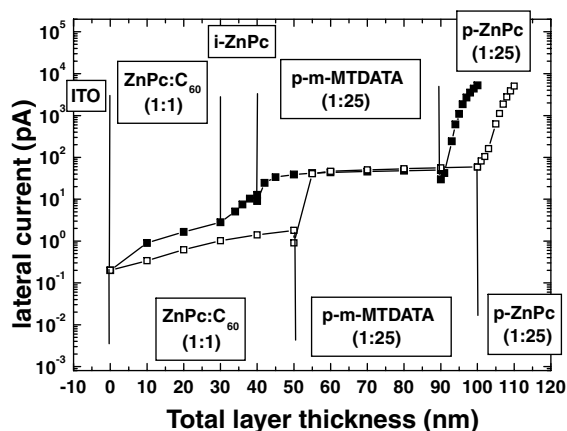


Fig. 2. The in-plane measured currents during evaporation process for two examples are shown. First sample (solid squares) has the layer sequence ITO/30 nm ZnPc: C_{60} blend/10 nm ZnPc/50 nm p-doped m-MTDATA/10 nm p-doped ZnPc. The second sample (open squares) has the layer sequence ITO/50 nm ZnPc: C_{60} blend/50 nm p-doped m-MTDATA/10 nm p-doped ZnPc.

such evaporation procedure are shown. The sample structures are also displayed. With this method, we are able to derive detailed information on each sample. In the present hetero-junction MIP-type structure (see Fig. 2), the most important feature is the steep increase of current right at the beginning of the evaporation of the doped layer, followed by a weak linear growth in current. We interpret the first part in terms of a diffusion of dopants into the undoped layer causing higher conductivity by transport of holes in ZnPc. Note that the conductivity of doped ZnPc is several orders of magnitude higher than for doped m-MTDATA at the same doping level [23]. The subsequent weak linear increase of conductance corresponds to the expected conductivity of the p-doped m-MTDATA layer.

3. Results and discussion

3.1. Contact behavior

3.1.1. Current voltage characteristics

The crucial requirements for solar cell performance are high carrier generation efficiency, good bipolar carrier transport, low recombination losses and minimum losses in free energy in all conversion steps involved. However, the potential of an organic photoactive layer with respect to these fundamental issues can not be fully exploited unless the interface behavior between different layers and at the contact electrodes is optimized. Even small discontinuities may have a strong impact on fill factor or short circuit current and will reduce the performance of the solar cells.

As reported previously [22], the *IV*-characteristics of various MIP-type diodes including p-doped m-MTDATA as a hole transport layer with a gold top contact show a non-ohmic behavior at forward voltages adjacent to the exponential part in the diode characteristics. This is true both for homo-junctions (undoped/p-doped m-MTDATA) [22] and hetero-junctions (undoped ZnPc/p-doped m-MTDATA or undoped ZnPc:C₆₀-blend/p-doped m-MTDATA). Additionally, the calculated current that should be reached at a certain positive bias voltages according to the bulk conductivity of the

doped transport layer has never been achieved. An ohmic contact, however, is an essential requirement. Consequently, all the interfaces were checked for their ohmic behavior by systematically testing various layer combinations, including different doping concentrations and preparation conditions. We found clear indications for a non-ohmic behavior of the top-evaporated gold electrode on p-doped m-MTDATA. This behavior, however, was not to be expected from the energy levels involved. After all, it was found that doped m-MTDATA forms an ohmic contact with ITO bottom contacts, even though ITO has a lower workfunction than gold. We therefore attribute this effect to a de-doping and/or a destruction of the very top part of the organic layer during the evaporation of the very hot gold atoms. Additionally, a build-up of a small barrier at the contact might explain the findings. This build-up would be coincident if the effective metal work function is different for the layer deposited onto the organics as compared to between a pure metal layer. Such an effect has been found for several systems and was attributed to doping or chemical reactions [25,26]. Moreover, the diffusion of hot gold atoms into the organic layer might affect the contact properties [26,27].

Extremely high doping levels of m-MTDATA close to the contact leads to slight improvement, but is still not sufficient for solar cell applications. A change of the gold deposition parameters also yields a slight improvement, however, the increase is only slightly above experimental scatter. Both results point at a destruction or reaction of gold with the dopand F₄-TCNQ. However, none of the mentioned procedures improved the contact properties up to the level required.

The problem can be overcome by inserting a thin interlayer of highly p-doped zinc-phthalocyanine. Fig. 3 shows the comparison of two samples with the layer sequence consisting of ITO/50 nm ZnPc (undoped)/300 nm m-MTDATA (p-doped with 4 mol%)/10 nm ZnPc (p-doped with 4 mol%, only for one sample)/Au. Dark and illuminated *IV* characteristics are shown. With the doped ZnPc interlayer, the forward-current at +1 V is increased by half an order of magnitude. Now, the current at forward bias fits extremely well to the model of a diode with an additional ohmic

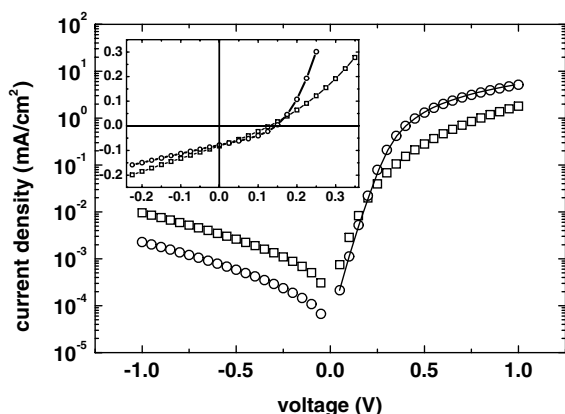


Fig. 3. Current–voltage characteristics of two MIP-type structures show the increased contact performance by introduction of a thin doped ZnPc layer (open circles). For comparison, the sample is shown without this ZnPc layer (open squares). The inset demonstrates the improved solar cell performance due to increased fill factor at 100 mW/cm² white light illumination.

series resistance (solid line) whereas the sample without the additional p-ZnPc layer behaves non-ohmic. The fitted series resistance of 0.01 Ωm² corresponds to a conductivity of approximately 3.5 × 10⁻⁷ S/cm. Similar values were measured for m-MTDATA doped with 4 mol% of F₄-TCNQ [22].

This approach, however, has a serious drawback: the ZnPc layer absorbs light, but does not contribute to the photocurrent. Therefore, the layer thickness has to be minimized. By a series of thickness variations, the optimum value was found to be close to 10 nm.

3.1.2. Impedance spectroscopy

By combined impedance spectroscopy (IS) and capacitance–voltage spectroscopy (CV) (see Figs. 4 and 5), we can obtain further insight into the origin of the non-ohmic contact behavior between evaporated gold and the p-doped m-MTDATA. A simple equivalent circuit model describes in principle the main features of the measured data. We compare again the two different sample structures of hetero-MIP-diodes without (I) and with (II) p-ZnPc interlayer at the gold contacts. In the IS, the samples differ mainly by the shape of the curves: for sample type (I), the capacitance

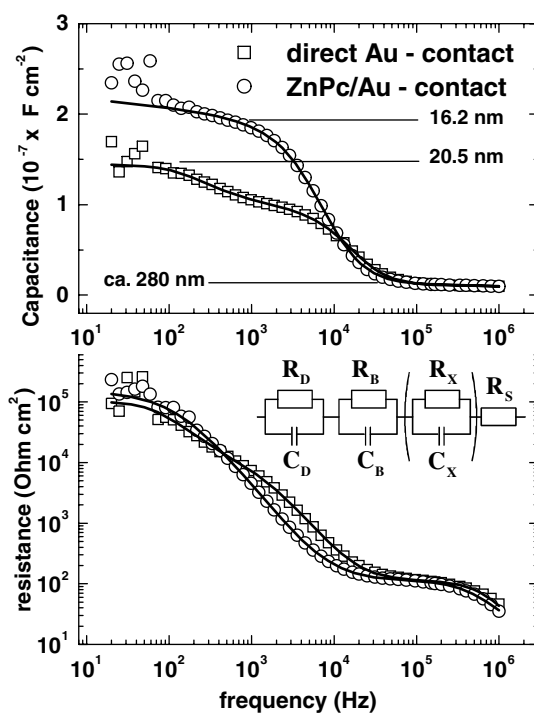


Fig. 4. Impedance spectra for sample types (I) and (II) at 0 V bias voltage. The solid lines represent the fit for the respective device types.

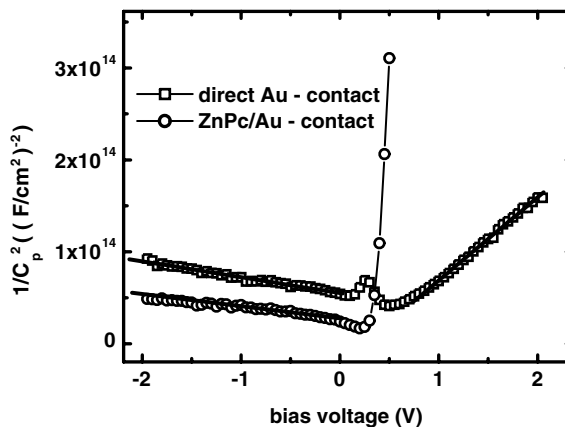


Fig. 5. Mott–Schottky plot for both sample types shown in Fig. 3 with and without ZnPc interlayer at the gold contact. The solid lines represent linear fits for corresponding voltage ranges according to Eq. (3).

drops in two steps with increasing frequency. The first step is between 100 and 500 Hz and the

second step between 10 and 50 kHz. We attribute these two steps to two independent relaxation processes within the sample. They feature two different time regimes suggesting two regions of different conductivity within the bulk. In comparison, sample type (II) shows only one step in capacitance at around 10 kHz. Moreover, the absolute difference in capacitance value at low frequencies is evident. This we attribute to slight differences in sample preparation that might occur by diffusion of dopants into the undoped layers. The formally calculated thicknesses corresponding to the capacitance values are depicted in Fig. 4 as well.

To make the evaluation of the shown data more quantitatively, the mentioned circuit model (given in Fig. 4) is built up equivalently to the device structure. Here, we assign a single RC-component to each of the deposited layers. It consists of mainly three parts: (1) an RC-component (R_D-C_D) for the depletion region including the undoped ZnPc layer (low conductivity–high relaxation time), (2) an RC-component (R_B-C_B) for the bulk (p-doped) layer (high conductivity–low relaxation time) and (3) a resistor (R_S) representing the series resistance. For sample type (I), an additional RC-component (R_X-C_X) has to be added to account for a low conductivity layer next to the gold top contact. By fitting the data with the above described circuit model using regular capacitors, the behavior cannot be fully satisfactorily described. The steady increase of capacitance with decreasing frequency at low frequencies and the smeared-out transitions cannot be reproduced with any equivalent circuit using regular capacitors. One rather has to use *distributed circuit elements* [28] that account for a distribution of energy states [29,30] or more probable a spatially distributed conductivity [28]. In the simplest case, a constant phase element (CPE) replaces

the regular capacitor in the circuit model. It represents a region of exponentially changed conductivity that may occur at non-abrupt interfaces. In Eq. (1), the general expression for a CPE is given [28,31,32].

$$Z(\omega)_{\text{CPE}} = \frac{1}{\omega_0 C_{\text{eff}} \left(i \frac{\omega}{\omega_0} \right)^\alpha} \quad (1)$$

Here, $Z(\omega)_{\text{CPE}}$ is the complex impedance, i the imaginary unit, C_{eff} the effective capacitance, ω_0 a characteristic frequency corresponding to the frequency of maximum capacitive contribution for each single relaxation, ω the circular frequency, and α ($0 \leq \alpha \leq 1$) a parameter which describes the degree of capacitive character. To give a more illustrative meaning to the parameter α , it can be written with some approximations as [28]:

$$\alpha \approx 1 - \frac{\delta}{d} \quad (2)$$

The parameter d represents the thickness of the actual layer and δ is the characteristic length wherein the conductivity drops to $1/e$ of the original value.

The fit parameters for both sample structures that have been deduced using this equivalent circuit model are listed in Table 1. Whereas for sample type (I), the third RC-component (R_X-C_X) is essential, a fit to sample type (II) can be reduced to only two RC-components and a series resistance. The corresponding fits to each measurement are depicted in Fig. 4 as solid lines. Both show only small deviations from the measured curves and demonstrate the ability of the applied model. As a plausibility check, the conductivities have been calculated for each layer. The conductivities are approximately 10^{-11} and 5×10^{-10} S/cm for depletion layer and the contact layer, respectively. The

Table 1

Fit parameters deduced by application of the equivalent circuit model shown in Fig. 4 using constant phase elements (CPE)

Sample	C_D [F/cm ²]	R_D [Ω cm ²]	C_X [F/cm ²]	R_X [Ω cm ²]	C_B [F/cm ²]	R_B [Ω cm ²]	R_S [Ω cm ²]
Without ZnPc contact	1.5×10^{-7}	1.1×10^5	3.9×10^{-7}	1.4×10^3	1.3×10^{-8}	83	3.2
With ZnPc contact	2.1×10^{-7}	3.4×10^5	–	–	1.3×10^{-8}	94	4.7

C: effective capacitance calculated from CPE-parameters. R: resistance. All resistance values are given within respect to the measured active area. For the sample type without the ZnPc layer, a satisfying fit is achieved only with an additionally RC-component (R_X-C_X) corresponding to a low conductivity layer at the non-ideal contact.

value for the doped bulk layer is about 3×10^{-7} S/cm, which is in good agreement with *IV* measurements and values, obtained directly from single layers in a coplanar geometry [22].

3.1.3. Capacitance–voltage spectroscopy

The existence of a low conductivity layer at the contact between doped m-MTDATA and gold is now established. However, its origin and the way it limits the contact is still unclear. To obtain more insight, we performed *CV* measurements, a method that is typically applied to reveal interface behavior and doping densities [33,34]. Here the capacitance (in parallel mode) is monitored at a constant frequency as a function of the bias voltage. Typically, the capacitance of the region of the lowest conductivity is measured at low frequencies. In our case, this is the capacitance of the depletion region including the undoped layer. According to the IS data (Fig. 4), the frequency is chosen to be 120 Hz. In Fig. 5, the *CV* measurements of the two sample structures are shown in the so-called Mott–Schottky plot. At reverse bias, the depletion layer extended by the nominally undoped ZnPc layer is seen for both sample structures. However, the nominal thickness of the intrinsic ZnPc (50 nm) is not reproduced. This points to a diffusion of dopants into the nominally undoped layer during evaporation of the hole transport layer (p-m-MTDATA), which has been observed in the monitored lateral current during evaporation as well (see Fig. 2). The measured value can vary between 20 and 30 nm for different samples, due to experimental errors of the thickness monitor and the evaporation conditions. Only at forward bias voltages, significant differences between the two types of samples show up. In structure (II), the depletion region breaks down followed by an abrupt drop of the capacitance approaching towards the geometric capacitance of the whole sample for higher voltages. Structure (I) however shows a completely different behavior. After break down of the depletion region, the capacitance increases again to a second maximum and then decreases gradually to a value corresponding to a thickness of around 30–40 nm.

This behavior can be explained as follows: by evaporation of Au on top of p-doped m-MTDATA, a small barrier is created resulting in a weakly depleted region that limits the current flow at forward bias. This implies also an effective work function of top-evaporated gold of less than 4.9 eV (estimated work function of doped m-MTDATA, having an ionization energy of 5.1 eV). The thickness of this depletion layer can be roughly explained by a classical Schottky contact. The active doping level can be derived from the slope of the Mott–Schottky plot according to

$$N_A = \frac{2}{\varepsilon A^2 \frac{d(1/C^2)}{dV}} \quad (3)$$

where N_A is the acceptor density, ε the dielectric constant, A the device area and $\frac{d(1/C^2)}{dV}$ the slope of the Mott–Schottky plot in the interesting voltage range. The value of 1×10^{18} S/cm found here is significantly lower than the nominal doping level.

We therefore conclude that, additionally to the small barrier, a de-doping effect occurs at the interface due to gold diffusion into the organic layer accompanied by destruction or chemical reaction of gold with the dopants. This results in a non-ohmic contact behavior. A detailed understanding of this de-doping process cannot be obtained within the methods used here.

The improved contact behavior by a thin p-doped ZnPc interlayer may be attributed to two points: first, ZnPc has a higher mobility than m-MTDATA and its doping efficiency is better [23]. Furthermore, ZnPc has a different morphology (polycrystalline, more stable) and the Zn atoms in the molecules might act as seeds for gold clusters. This may lead to a lower diffusion of gold atoms into the organic layer and prevent the de-doping effect. The improved contact behavior has a strong impact on the solar cell performance, too. The most important improvement is clearly observed for the fill factor (change from 29% to 36%, see inset in Fig. 3).

3.2. Donor–acceptor blends as active layer

3.2.1. Photovoltaic characterization

In Fig. 6, the influence of the photoactive layer on the photovoltaic performance of MIP-type

diodes is shown. For the cells with ZnPc as active layer, only the principle can be demonstrated. Both the short circuit current (I_{SC}) and the open circuit voltage (V_{OC}) are by far too low to result in a good solar cell. The short circuit current is mainly limited by low charge carrier generation efficiency in ZnPc or at the interface ITO/ZnPc, respectively and V_{OC} depends strongly on pre-treatment of the ITO surface.

The performance is improved drastically when we implement a donor–acceptor blend. According to various publications, such blends promise higher charge carrier generation, broader absorption range and a quasi bi-polar charge transport [18–21,35–37]. Therefore, we replace the *i*-ZnPc layer in the MIP structure by the mixture of ZnPc and the fullerene C_{60} with a molar ratio of one by one. This system has been investigated previously [2] and serves here as a model system for a manifold of combinations of donor–acceptor blends. In Fig. 6, we compare IV characteristics in the dark and under illumination with 100 mW/cm^2 white light. The sample structure is kept unchanged, except for the photoactive layer which consists of either neat ZnPc or a ZnPc: C_{60} blend. The dark IV curves behave rather similarly; however, the illuminated IV 's point out the enormous improvement in charge carrier generation efficiency when using

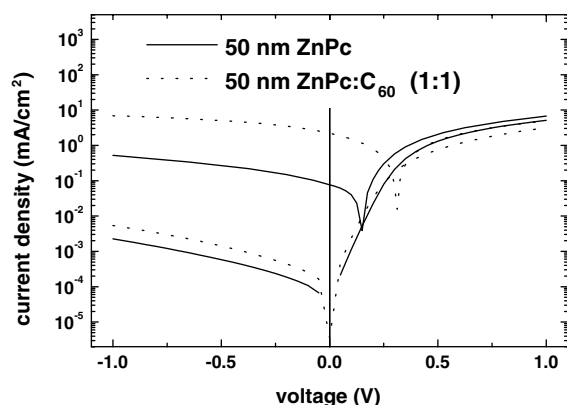


Fig. 6. Current voltage characteristics in the dark and under 100 mW/cm^2 white light illumination for two MIP-type structures with the layer sequence ITO/photoactive layer/*m*-MTDATA (300 nm, 4 mol% doping)/ZnPc (10 nm, 4 mol% doping)/Au where the photoactive layer is 50 nm pure ZnPc (solid lines) or 50 nm ZnPc: C_{60} blend with a molar ratio of one by one (dotted line).

blend layers. Here, the high series resistance due to the 300 nm thick p-doped *m*-MTDATA layer is the main limitation for the short circuit current. Nevertheless, the extremely high charge carrier generation efficiency is demonstrated in an impressive way. In order to reduce the influence of series resistance, the thickness of p-doped *m*-MTDATA is decreased from 300 to 50 nm. As can be seen in Fig. 7, this already leads to an obvious raise of I_{SC} from 2.0 mA/cm^2 (cell type A) to 3.9 mA/cm^2 (cell type B). Additionally, the fill factor changes from 0.25 to 0.36, but is still limited by the series resistance present. The open circuit voltage stays unchanged. Thinner layers would further decrease the resistance, but cause lower reproducibility and stability due to higher probability of short circuits. A higher doping level is not efficient enough to increase the conductivity to the necessary amount. In this series of samples, we used an active layer thickness of only 30 nm ZnPc: C_{60} . Thicknesses of larger than 50 nm ZnPc: C_{60} blend (molar ratio 1:1) tend to limit the charge carrier transport in the cells due to considerably lower mobilities in blend layers, as compared to single

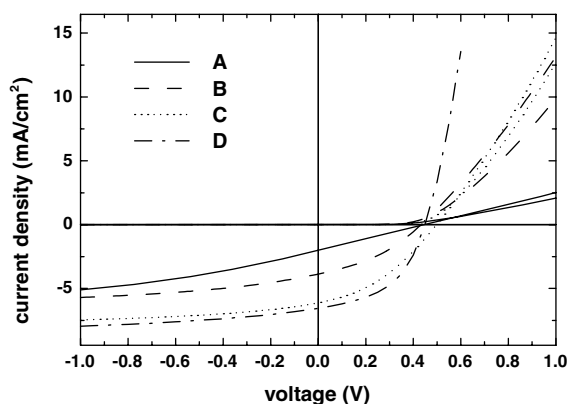


Fig. 7. Evolution of MIP-type test structures during improving of structure and material combination towards higher solar cell efficiencies. Shown are dark and illuminated current voltage characteristics at an illumination intensity of 100 mW/cm^2 white light. (A) ITO/30 nm ZnPc: C_{60} /300 nm p-*m*-MTDATA/10 nm p-ZnPc/Au. (B) ITO/30 nm ZnPc: C_{60} /50 nm p-*m*-MTDATA/10 nm p-ZnPc/Au. (C) ITO/30 nm ZnPc: C_{60} /10 nm ZnPc/50 nm p-*m*-MTDATA/10 nm p-ZnPc/Au. (D) ITO/30 nm ZnPc: C_{60} /10 nm ZnPc/50 nm p-MeO-TPD/10 nm p-ZnPc/Au.

component layer systems [38]. Due to the slow transport, the recombination of photogenerated carriers becomes more likely. A study of charge transport in such kind of blends will be presented elsewhere. In order to further improve the solar cell performance, we looked for a way to increase the absorption and thus the I_{SC} , without limiting the charge carrier transport. It is known that ZnPc is able to transport holes quite efficiently, even without p-type doping due to the reasonably high mobility [23]. Moreover, excitons created in ZnPc are able to diffuse about 5–10 nm [4] to the interface ZnPc:C₆₀/ZnPc where they are separated and contribute to the photocurrent. We thus implemented an additional interlayer of 10 nm neat ZnPc in between the ZnPc:C₆₀ blend and the wide-gap transport layer of p–m-MTDATA. Here, the favorable effect of wide-gap transport layers to reflect the excitons at the interface is used as well. The result can be seen in Fig. 7 (cell type C). The significant enhancement of photocurrent suggest a reasonable contribution of the neat ZnPc layer. The increase of the saturation current at a reverse bias voltage of –1 V from 5.7 to 7.5 mA/cm² approximately corresponds to the additional absorption of the introduced ZnPc layer. Therefore, we conclude that nearly the whole ZnPc contributes to the photocurrent.

Despite the improved I_{SC} , the solar cells still suffer from a too low fill factor. Obviously, it is limited by the series resistance caused by the low conductivity of the doped transport layer (m-MTDATA). MeO-TPD, a methoxy-substituted derivative of TPD has been used to replace m-MTDATA as a hole transport material. Assuming a similar mobility to TPD, its mobility should be about one to two orders of magnitude higher than for m-MTDATA [39]. Due to the electron-pushing methoxy substituents, its ionization energy is lowered as compared to TPD. Thus, doping by our standard dopant F₄-TCNQ becomes efficient and the conductivity reaches values as high as 1×10^{-5} S/cm at a doping concentration of 4 mol%. Correspondingly, the lower series resistance improves the fill factor from 37% to 49%, where V_{OC} and I_{SC} stay unchanged, and enables higher solar cell power efficiencies of up to 1.44% at 100 mW/cm² white light illumination (Fig. 7) (cell type D). Solar

Table 2

Overview of solar cell performance parameters open circuit voltage (V_{OC}), short circuit current (I_{SC}), fill factor (FF) and power efficiency (η) for all MIP-type structures shown in Fig. 7

Structure	V_{OC} (V)	I_{SC} (mA/cm ²)	FF	η (%)
A	0.44	2.0	0.25	0.22
B	0.43	3.9	0.36	0.60
C	0.50	6.12	0.37	1.13
D	0.45	6.55	0.49	1.44

All parameters are determined under illumination with 100 mW/cm² white light.

cell performance parameter for all cell types are summarized in Table 2 for comparison.

3.2.2. Internal and external quantum efficiencies

High internal quantum efficiencies are an important step towards highly efficient organic solar cells. By using wide-gap transport layers, our approach ensures that absorption takes place in the active region only, permitting high internal quantum efficiencies. To determine those, we measured UV/VIS reflection in a setup of quasi-perpendicular incident beam geometry. As an example, the data are shown in Fig. 8 for the final MIP-type structure with pure ZnPc adjacent to the blended layer. To calculate the total absorption in the layer structure, we measured two samples. First, the reflection data are taken from the complete structure (glass/ITO/30 nm ZnPc:C₆₀/10 nm ZnPc/50 nm m-MTDATA/10 nm ZnPc/40 nm gold). Next, we prepared a sample of the transport layers only, which consists of glass/ITO/50 nm m-MTDATA/10 nm ZnPc/40 nm gold (dotted line). This way, we are able to exclude the thin ZnPc layer close to gold electrode (which does not contribute to the photocurrent) for the estimation of the internal quantum efficiency of the active layer system. Additionally, we can exclude the effect of reflected light at the glass–air interface and further interfaces as well as unknown losses due to non-ideal reflection at the metal back contact. The difference of the two graphs in Fig. 8 yields the absorbance in the active region versus the wavelength. The maximum is around 40% at the peak absorption of ZnPc. Negative values at about 530 nm are due to slightly different thicknesses of the two samples and represent the actual error of this method. By taking these data in combination with

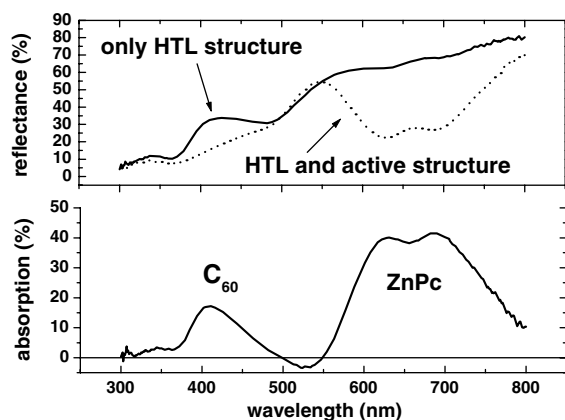


Fig. 8. Measured reflectance and calculated absorbance spectra. The upper diagram shows the reflectance of the complete MIP-type structure (solid line: glass/ITO/30 nm ZnPc:C₆₀/10 nm ZnPc/50 nm m-MTDATA/10 nm ZnPc/40 nm gold) and the reduced structure without the active layers (dotted line: glass/ITO/50 nm m-MTDATA/10 nm ZnPc/40 nm gold), measured in quasi perpendicular incident beam geometry. The lower diagram depicts the calculated total absorbance.

the AM 1.5 sun spectra at 100 mW/cm², we estimate that the light being absorbed in the active layers corresponds to a photocurrent of about 5.8 mA/cm² assuming 100% internal quantum efficiency (IQE). In comparison with the short circuit current of about 6.5 mA/cm², we find a slight discrepancy suggesting a IQE of 100%. Direct measurement of incident photon to current efficiency at a wavelength of 625 nm, corresponding to the peak absorption, yields an external quantum efficiency (EQE) of about 25–30%. In combination with the effective absorption (see Fig. 8), we conclude that the internal quantum efficiency is close to 70% at peak absorption (625 nm). The difference between the measured and calculated photocurrent is attributed to a spectral mismatch between the used light source and the AM 1.5 sun spectra. A more detailed investigation of action spectra or incident photon to current efficiency (IPCE) will be presented in a future publication.

3.3. Inverted MIP-type structures

At the beginning of this article, we referred to some advantages of organic solar cells with doped wide-gap transport layers. In fact, it was shown

that metal evaporation of top contact electrodes is always a critical point during the preparation of thin samples [26,27]. By varying the deposition conditions, one may eliminate or reduce some problems. Nevertheless, it has been shown that hot metal atoms penetrate into the organic layers. Interdiffusion, doping effects, chemical reactions or an inert behavior have been reported [26,27,40] for metal on organic contacts depending on metal/organic combination.

In the structures studied here, in particular the active donor–acceptor blend might be extremely sensitive to metal atoms or clusters. These can quench the excitons created or act as recombination centers for the charge carriers. Furthermore, one might imagine that the first few nanometers of the blend show a more or less quasi-metallic behavior and do not contribute to the photocurrent. For instance, Owens et al. [40] reported on diffusion of aluminium atoms into C₆₀ layers and a donor-like behavior of Al in C₆₀. Finally, a kind of

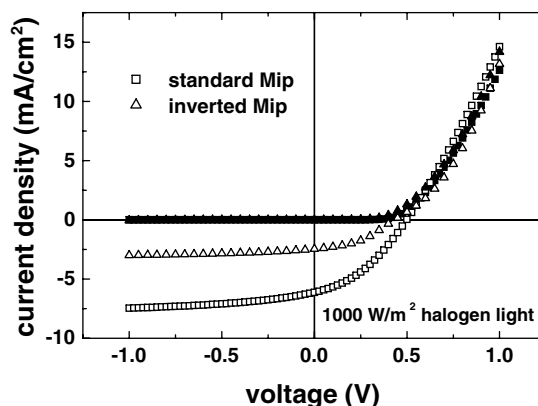


Fig. 9. Current voltage characteristics in the dark (filled symbols) and under illumination with 100 mW/cm² white light (open symbols). The diagram shows the comparison of a standard MIP-type structure (open squares) and an inverted structure (open triangles). In the standard structure (squares: glass/ITO/30 nm ZnPc:C₆₀/10 nm ZnPc/50 nm p-doped m-MTDATA/10 nm p-doped ZnPc/40 nm gold), the active layer is separated from the vacuum deposited metal electrode by the doped transport layer, whereas in the inverted MIP diode (triangles: glass/ITO/10 nm p-doped ZnPc/50 nm p-doped m-MTDATA/10 nm ZnPc/30 nm ZnPc:C₆₀/50 nm aluminium), the active layer is directly exposed to evaporated metal electrode. Note that the polarity of the inverted MIP has been changed for the reason of comparability.

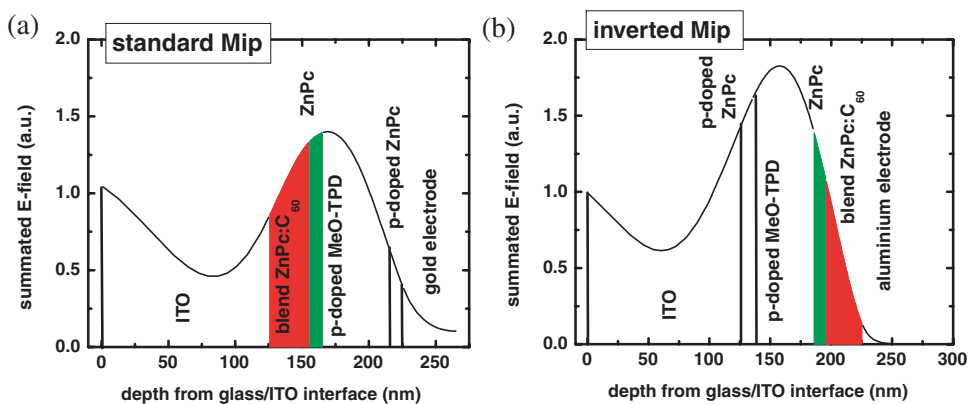


Fig. 10. Optical simulation according to transfer matrix formalism of standard (a) and inverted (b) MIP structure. Given are the summated optical E-field of both device.

n-type doping of the blend ZnPc:C₆₀ close to the contact is rather probable. In fact, optical thin film effects will cause a large drop in current also. This is due to lowered optical field intensity close to the metal contact. In any case, the introduction of an doped wide-gap transport layer between the active layer and the metal is a favorable solution to prevent these effects.

Fig. 9 demonstrates how dramatic the negative influence of a metal contact directly on the active layer is. Here we compare a standard MIP diode (see previous section) and an inverted MIP diode where the organic layer sequence is inverted (p-doped/intrinsic/metal) and the blended layer faces to a top-evaporated aluminium contact. Consequently, the electric field and the charge transport is in the opposite way. For reason of comparability the polarity has been changed in Fig. 9. Open circuit voltage and fill factor remain roughly unchanged, but the short circuit current of the inverted cell is decreased by more than a factor of two. The difference is even more significant for the saturation currents at reverse bias (7.5 versus 3.0 mA/cm²) where the impact of remaining series resistance and of recombination processes is low. To extract the main reason for the observed current drop, we have carried out optical simulations on both structures based on the so-called transfer matrix formalism (TMF) [41,42]. As a result, the optical field distribution is shown in Fig. 10. Even though the device has not been tuned to optimum field distribution for the standard structure (see

Fig. 10(a)) the difference between both structures is clearly seen. From the calculated number of absorbed photons within the active layers (blend and undoped ZnPc) at an illumination of 100 mW/cm² AM 1.5 light, we get maximum photocurrents of 9.3 and 5.0 mA/cm² for the standard and the inverted structure, respectively. This trend is confirmed by the measured saturation currents of 7.5 and 3.0 mA/cm², respectively. The deviation in the absolute values between simulation and measurement may be caused by a limited quantum efficiency of carrier generation in the neat ZnPc layer or simply by the spectral mismatch between the AM 1.5 spectrum and the light of the halogen lamp used here. Nevertheless, we can conclude that optical thin film effects play the dominant role. However, as the observed difference between the two structures seems to be larger than it is to be expected from optical effects alone, additional effects like metal induced damages or interdiffusion cannot be excluded, either.

4. Conclusion

We have demonstrated the importance of device architecture optimization, the proper choice of materials and their combination for the optimization of highly efficient organic solar cells. This study is a step towards PIN type high efficiency solar cells with optimized structure. The contact properties between doped wide-gap transport layer

and gold electrode were investigated and improved by adding a thin doped ZnPc layer. Within an evolution of Schottky type cells (MIP), the power efficiency was raised by more than a factor of six, reaching 1.44% at 100 mW/cm² white light illumination. Hereby, we propose a new type of cell taking advantage of both the bulk hetero-junction concept (limited by carrier transport) and double layer concept (limited by exciton diffusion to the interfaces). Finally, we have demonstrated the essential role of wide-gap transport layers to avoid the detrimental influence of metal interdiffusion and profit from thin film optical effects.

Acknowledgements

The authors thank M. Koch for material purification and technical assistance and the German Secretary for Education and Research (BMBF, FKZ 01SF0027) for financial support.

References

- [1] S.E. Shaheen, R. Radspinner, N. Peyghambarian, G.E. Jabbour, *Appl. Phys. Lett.* 79 (18) (2001) 2996.
- [2] D. Gebeyehu, B. Maennig, J. Drechsel, K. Leo, M. Pfeiffer, *Sol. Energy Mater. Sol. Cells* 79 (2003) 81.
- [3] S.E. Shaheen, C.J. Brabec, N.S. Sariciftci, F. Padinger, T. Fromherz, J.C. Hummelen, *Appl. Phys. Lett.* 78 (6) (2001) 841.
- [4] P. Peumans, S.R. Forrest, *Appl. Phys. Lett.* 79 (1) (2001) 126.
- [5] P. Peumans, S.R. Forrest, *Appl. Phys. Lett.* 80 (2) (2002) 338.
- [6] C.J. Brabec, N.S. Sariciftci, J.C. Hummelen, *Adv. Funct. Mater.* 11 (1) (2001) 15.
- [7] C.W. Tang, *Appl. Phys. Lett.* 48 (2) (1986) 183–185.
- [8] A. Yakimov, S.R. Forrest, *Appl. Phys. Lett.* 80 (9) (2002) 1667.
- [9] A. Twarowski, *J. Chem. Phys.* 77 (9) (1982) 4698.
- [10] M. Hiramoto, K. Ihara, M. Yokoyama, *Jpn. J. Appl. Phys. Part 1* 34 (7B) (1995) 3803.
- [11] H. Laurs, G. Heiland, *Thin Solid Films* 149 (1987) 129.
- [12] Y. Yamamoto, K. Yoshino, Y. Inuishi, *J. Phys. Soc. Jpn.* 47 (6) (1979) 1887.
- [13] K. Kuhnke, R. Becker, M. Epple, K. Kern, *Phys. Rev. Lett.* 79 (17) (1997) 3246.
- [14] M. Pfeiffer, S.R. Forrest, K. Leo, M.E. Thompson, *Adv. Mater.* 14 (22) (2002) 1633.
- [15] X. Zhou, J. Blochwitz, M. Pfeiffer, A. Nollau, T. Fritz, K. Leo, *Adv. Funct. Mater.* 11 (4) (2001) 310.
- [16] X. Zhou, M. Pfeiffer, J.S. Huang, J. Blochwitz-Nimoth, D.S. Qin, A. Werner, J. Drechsel, B. Maennig, K. Leo, *Appl. Phys. Lett.* 81 (5) (2002) 922.
- [17] J. Huang, M. Pfeiffer, A. Werner, J. Blochwitz, Sh. Liu, K. Leo, *Appl. Phys. Lett.* 80 (2002) 139.
- [18] T. Tsuzuki, Y. Shirota, J. Rostalski, D. Meissner, *Sol. Energy Mater. Sol. Cells* 61 (2000) 1.
- [19] D. Meissner, J. Rostalski, *Synth. Met.* 121 (2001) 1551.
- [20] J. Rostalski, D. Meissner, *Sol. Energy Mater. Sol. Cells* 61 (2000) 87.
- [21] M.A. Loi, P. Denk, H. Neugebauer, C. Brabec, N.S. Sariciftci, A. Gouloumis, P. Vazquez, T. Torres, *AIP Conf. Proc.* 633 (2002) 488.
- [22] J. Drechsel, M. Pfeiffer, X. Zhou, A. Nollau, K. Leo, *Synth. Met.* 127 (2002) 201.
- [23] B. Maennig, M. Pfeiffer, A. Nollau, X. Zhou, P. Simon, K. Leo, *Phys. Rev. B: Condens. Matter* 64 (2001) 195208.
- [24] R. Schmechel, *Phys. Rev. B: Condens. Matter* 66 (2002) 235206.
- [25] I.G. Hill, A. Rajagopal, A. Kahn, *J. Appl. Phys.* 84 (6) (1998) 3236.
- [26] C. Shen, A. Kahn, *J. Appl. Phys.* 90 (2001) 4549.
- [27] A. Thran, T. Strunskus, V. Zaporojtchenko, F. Faupel, *Appl. Phys. Lett.* 81 (2) (2002) 244.
- [28] J.R. Macdonald, *Impedance Spectroscopy—Emphasizing Solid Materials and Systems*, John Wiley & Sons Inc., New York, 1987.
- [29] W.E. Spear, P.G. Le Comber, A.J. Snell, *Philos. Mag.* B 38 (1978) 303.
- [30] A.J. Snell, K.D. Mackenzie, P.G. Le comber, W.E. Spear, *Philos. Mag.* B 40 (1979) 1.
- [31] H. Göhr, *Ber. Bunsen. Phys. Chem.* 85 (1981) 274.
- [32] H. Göhr, J. Schaller, C.-A. Schiller, *Electrochim. Acta* 38 (1993) 1961.
- [33] G. Paasch, S. Scheinert, *Synth. Met.* 122 (1) (2001) 145.
- [34] J. Scherbel, P.H. Nguyen, G. Paasch, W. Brtting, M. Schwoerer, *J. Appl. Phys.* 83 (10) (1998) 5045.
- [35] G. Ruani, C. Fontanini, M. Murgia, C. Taliani, *J. Chem. Phys.* 116 (4) (2002) 1713.
- [36] M. Hiramoto, K. Suemori, M. Yokoyama, *Jpn. J. Appl. Phys. Part 1* 41 (4B) (2002) 2763.
- [37] T. Stuebinger, W. Bruetting, *J. Appl. Phys.* 90 (7) (2001) 3632.
- [38] B. Männig et al., The mobilities of blended layers ZnPc:C60 have been measured in a field effect transistor geometry and show considerably lower values than mobilities of neat layers of ZnPc or C60, to be published.
- [39] Y. Shirota, *J. Mater. Chem.* 10 (1) (2000) 1.
- [40] D.W. Owens, C.M. Aldao, D.M. Poirier, J.H. Weaver, *Phys. Rev. B: Condens. Matter* 51 (1995) 17068.
- [41] L.A.A. Pettersson, L.S. Roman, O. Inganas, *J. Appl. Phys.* 86 (1) (1999) 487.
- [42] H. Hoppe, N. Arnold, N.S. Sariciftci, D. Meissner, *Sol. Energy Mater. Sol. Cells* 80 (2003) 105.